Stability of Metal Nanowires at Ultrahigh Current Densities

C.-H. Zhang, J. Bürki, and C. A. Stafford

Department of Physics, University of Arizona, 1118 E. 4th Street, Tucson, AZ 85721
(Dated: November 4, 2004)

We develop a generalized grand canonical potential for the ballistic nonequilibrium electron distribution in a metal nanowire with a finite applied bias voltage. Coulomb interactions are treated in the self-consistent Hartree approximation, in order to ensure gauge invariance. Using this formalism, we investigate the stability and cohesive properties of metallic nanocylinders at ultrahigh current densities. A linear stability analysis shows that metal nanowires with certain *magic conductance values* can support current densities up to $10^{11}\mathrm{A/cm}^2$, which would vaporize a macroscopic piece of metal. This finding is consistent with experimental studies of gold nanowires. Interestingly, our analysis also reveals the existence of reentrant stability zones—geometries that are stable only under an applied bias.

I. INTRODUCTION

Metal nanowires have been the subject of many experimental and theoretical studies, both for their novel properties and potential applications (see Ref. 1 for a review of the field). One of the most remarkable properties of metal nanowires is their ability to support extremely high current densities without breaking apart or vaporizing.[2,3,4,5,6,7,8] For noble metals, experiments can be carried out in air, and the first few peaks in conductance histograms can withstand applied voltages as high as one Volt, and even two Volts for the first peak, corresponding to one conductance quantum $G_0 = 2e^2/h$. Let us estimate the corresponding current density: For a ballistic metallic conductor in the form of a cylinder of radius R, the electrical conductance G is given approximately by the Sharvin formula $G \simeq G_0(k_F R/2)^2$, where k_F is the Fermi wavevector. Therefore the current density at applied voltage V is

$$j = \frac{GV}{\pi R^2} \simeq \frac{k_F^2 G_0 V}{4\pi} = \frac{3nev_F}{8} \times \frac{eV}{\varepsilon_F}, \qquad (1)$$

where n is the number density of conduction electrons, v_F is the Fermi velocity, and ε_F is the Fermi energy. For an applied bias of a few Volts, the factor eV/ε_F is of order unity, and the current density is of order $10^{11}\mathrm{A/cm}^2$. Such high current densities would vaporize a macroscopic wire, thus prompting questions on the reason for the remarkable stability of metal nanowires.

The first part of the answer to this question is that metal nanowires are typically shorter than the mean-free path L_{in} for inelastic scattering, so that the conduction electrons can propagate through the wire without generating excitations such as phonons[8] that heat the wire. Instead, most of the dissipation takes place in the macroscopic contacts for the outgoing electrons. However, the absence of equilibration of the electron distribution within the nanowire raises another, more fundamental, question: What is the effect of a highly nonequilibrium electron distribution on the stability of a metal nanowire, given that the conduction electrons play a dominant role in the cohesion of metals? That is the question to which the present article is devoted.

Under a finite bias, the scattering states of right- and left-moving electrons in a nanowire are populated differently, even if there is no inelastic scattering within the wire. An adequate treatment of the electron-electron interactions is crucial to correctly describe this nonequilibrium electron distribution. Some studies of transport[9,10] and cohesion[11] in metal nanowires at finite bias did not include electron-electron interactions, so that the calculated transport and energetics depended separately on both the left and right chemical potentials μ_+ and μ_-, thus violating the *gauge invariance* condition: The calculated physical quantities should depend only on the voltage difference $eV = \mu_+ - \mu_-$, and should be invariant under a global shift of the electrochemical potential, since the total charge is conserved.[12] A self-consistent formulation of transport and cohesion at finite bias has recently been developed based on *ab initio* and tight-binding methods.[7,13,14,15,16] These computational techniques are particularly well-suited to the study of atomic chains, but can become intractable for larger nanostructures. An analytical approach to this problem is needed to study the interesting mesoscopic effects[17,18] which occur in systems intermediate in size between the macroscopic and the atomic scale.

In this paper, we extend our continuum model[18,19,20,21,22,23,24,25] of simple metal nanowires to treat the ballistic nonequilibrium electron distribution at finite bias. Coulomb interactions are included in the self-consistent Hartree approximation, which is adequate to ensure gauge invariance. For a system out of equilibrium, there is no general way to define a thermodynamic free energy. By assuming that the electron motion is ballistic, however, the energetics of the biased system can still be described by a nonequilibrium free energy,[26] which can be used to study the stability and cohesion of nanowires at finite bias. We find that for simple, monovalent metals, cylindrical nanowires with certain *magic conductance values*, $G/G_0 = 1, 3, 6, 12, 17, 23, 34, 42, \ldots$, can support current

densities up to $10^{11} \mathrm{A/cm^2}$. Our finding is consistent with experimental results for gold nanocontacts[2,3,4,5,6,7] ($G < 5G_0$) and atomic chains[8] ($G \simeq G_0$), but implies that the magic wires with $G > 5G_0$ are also extremely robust. Furthermore, we predict a number of nanowire geometries that are stable only under an applied bias.

This paper is organized as follows: In Sec. II, we develop a formalism to describe the nonequilibrium thermodynamics of a mesoscopic conductor at finite bias. In Sec. III, we apply this formalism to quasi-one-dimensional conductors, and obtain gauge-invariant results for the Hartree potential, grand canonical potential, and cohesive force of metal nanocylinders at finite bias. In Sec. IV, we perform a linear stability analysis of metal nanocylinders at finite bias, the principal result of the paper. Section V presents some discussion and conclusions. Details of the stability calculation are presented in Appendix A.

II. SCATTERING APPROACH TO NONEQUILIBRIUM THERMODYNAMICS

We consider a metallic mesoscopic conductor connected to two reservoirs at common temperature $T \equiv (k_B\beta)^{-1}$, with respective electrochemical potentials $\mu_{\pm} = \varepsilon_F + eV_{\pm}$, where ε_F is the chemical potential for electrons in the reservoirs at equilibrium, e is the electron charge, and $V_{+(-)}$ is the voltage at the left(right) reservoir (see Fig. 1). While there is no general prescription for constructing a free energy for such a system out of equilibrium, it is possible to do so based on scattering theory[26] if inelastic scattering can be neglected, i.e., if the length L of the conductor satisfies $L \ll L_{\mathrm{in}}$. In that case, scattering states within the conductor populated by the left(right) reservoir form a subsystem in equilibrium with that reservoir. Dissipation only takes place for the outgoing electrons within the reservoir where they are absorbed. Treating electron-electron interactions in mean-field theory, it is then possible to define a nonequilibrium grand canonical potential Ω of the system,

$$\Omega[\mu_+, \mu_-, U(\vec{r})] = \Omega_0[\mu_+, \mu_-, U(\vec{r})]$$
$$- \frac{1}{2} \int d^3r \, [\rho_-(\vec{r}) + \rho_+(\vec{r})]U(\vec{r}), \quad (2)$$

where Ω_0 describes independent electrons moving in the mean field U, $\rho_{\pm}$ are the number densities of electrons($-$) and of ionic background charges($+$), and the second term on the r.h.s. of Eq. (2) corrects for double-counting of interactions in Ω_0. Since the electrons injected from the left and right reservoirs are independent, aside from their interaction with the mean field, Ω_0 is given by the sum

$$\Omega_0[\mu_+, \mu_-, U(\vec{r})] = \sum_{\alpha=\pm} \Omega_\alpha[\mu_\alpha, U(\vec{r})], \quad (3)$$

where

$$\Omega_\alpha[\mu_\alpha, U] = -k_B T \int dE \, g_\alpha(E) \ln\left(1 + e^{-\beta(E-\mu_\alpha)}\right) \quad (4)$$
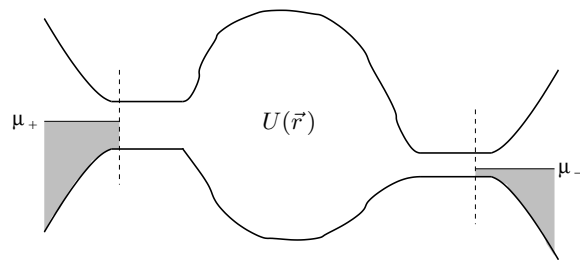

FIG. 1: Schematic depiction of a mesoscopic conductor connected to two reservoirs with respective electrochemical potentials μ_+ and μ_-. Within mean-field theory, the electronic scattering problem reduces to that of independent electrons moving in the self-consistent confinement potential $U(\vec{r})$.

is the grand canonical potential of independent electrons moving in the potential U, in equilibrium with reservoir α, and the *injectivity*[26,27,28]

$$g_\alpha(E) = \frac{1}{4\pi i} \sum_\gamma \mathrm{Tr}\left\{ S_{\gamma\alpha}^\dagger \frac{\partial S_{\gamma\alpha}}{\partial E} - \frac{\partial S_{\gamma\alpha}^\dagger}{\partial E} S_{\gamma\alpha} \right\} \quad (5)$$

is the partial density of states of electrons injected by reservoir α. Here $S_{\gamma\alpha} = S_{\gamma\alpha}[E, U(\vec{r})]$ is the submatrix of the electronic scattering matrix describing electrons injected from reservoir α and absorbed by reservoir γ, and is a functional of the mean-field potential.

The number density $\rho_-(\vec{r})$ of the conduction electrons is

$$\rho_-(\vec{r}) = \frac{\delta\Omega_0}{\delta U(\vec{r})} = \sum_{\alpha=\pm} \int dE \, g_\alpha(\vec{r}, E) f(E, \mu_\alpha), \quad (6)$$

where $f(E, \mu) = (1 + \exp[\beta(E - \mu)])^{-1}$ is the Fermi-Dirac distribution function, and

$$g_\alpha(\vec{r}, E) = -\frac{1}{4\pi i} \sum_\gamma \mathrm{Tr}\left\{ S_{\gamma\alpha}^\dagger \frac{\delta S_{\gamma\alpha}}{\delta U(\vec{r})} - \frac{\delta S_{\gamma\alpha}^\dagger}{\delta U(\vec{r})} S_{\gamma\alpha} \right\} \quad (7)$$

is the *local partial density of states*[26,27,28] for electrons injected from reservoir α. In Eqs. (6) and (7), $\delta/\delta U(\vec{r})$ denotes the functional derivative.

The mean-field potential U is determined in the Hartree approximation by

$$U(\vec{r}) = \int d^3r' \, V(\vec{r} - \vec{r}')\delta\rho(\vec{r}'), \quad (8)$$

where $\delta\rho(\vec{r}) = \rho_-(\vec{r}) - \rho_+(\vec{r})$ is the local charge imbalance in the conductor and $V(\vec{r}) = e^2/|\vec{r}|$ is the Coulomb potential. The Hartree potential depends on the electrochemical potentials of the left and right reservoirs.

The whole formalism (2)–(7) is very similar for any mean-field potential that is a local functional of the electron density,[13] but we choose to work with the Hartree potential for simplicity. The exchange and correlation contributions to the mean field are taken into account

in the present analysis only macroscopically,[21] by fixing the background density ρ_+ to its bulk value. Throughout this paper, we assume $\rho_+ = k_F^3/3\pi^2 = $ const. within the conductor (jellium model).

III. QUASI-ONE-DIMENSIONAL LIMIT

Equations (2)–(8) provide a set of equations at finite bias that have to be solved self-consistently. For a conductor of arbitrary shape, these equations may be quite difficult to solve. We therefore restrict our consideration in the following to quasi-one-dimensional nanoconductors, with axial symmetry about the z-axis. The shape of the conductor is specified by its radius $R(z)$ as a function of z, and we assume $R(z) \ll L$. For such a quasi-one-dimensional geometry, we can approximately integrate out the transverse coordinates, replacing the Coulomb potential by an effective one-dimensional potential

$$V(z, z') = \frac{e^2}{[(z-z')^2 + \frac{\eta}{2}(R^2(z) + R^2(z'))]^{1/2}}, \quad (9)$$

where η is a parameter of order unity. The longitudinal potential $V(z, z')$ has to be supplemented with a transverse confinement potential, which we take as a hard wall at the surface of the wire.[29] As a consistency check, our final results for the stability and cohesion are independent of the value of η chosen in the effective Coulomb potential.

With this form of the Coulomb potential, the mean field $U(z)$ becomes a function of the longitudinal coordinate only, and Eqs. (2)–(8) reduce to a series of one-dimensional integral equations, which are much more tractable. The grand canonical potential of a quasi-cylindrical wire of length L is

$$\Omega[\{\mu_\pm\}, R(z), U(z)] = \Omega_0[\{\mu_\pm\}, R(z), U(z)]$$
$$- \frac{1}{2}\int_0^L dz\,[\rho_-(z) + \rho_+(z)]U(z), \quad (10)$$

where Ω_0 is still given by Eqs. (3)–(5), with $\Omega_\alpha = \Omega_\alpha[\mu_\alpha, R(z), U(z)]$. Here

$$\rho_-(z) = \frac{\delta\Omega_0}{\delta U(z)} = \sum_{\alpha=\pm}\int dE\, g_\alpha(z, E)f(E, \mu_\alpha) \quad (11)$$

is the linear density of conduction electrons, where

$$g_\alpha(z, E) = -\frac{1}{4\pi i}\sum_\gamma \mathrm{Tr}\left\{S_{\gamma\alpha}^\dagger \frac{\delta S_{\gamma\alpha}}{\delta U(z)} - \frac{\delta S_{\gamma\alpha}^\dagger}{\delta U(z)}S_{\gamma\alpha}\right\} \quad (12)$$

is the injectivity of a circular slice of the conductor at z. The scattering matrix $S = S[E, R(z), U(z)]$ is now a functional of $R(z)$ and $U(z)$. The linear density of

positive background charges is

$$\rho_+(z) = \frac{k_F^3 R(z)^2}{3\pi} - \frac{k_F^2 R(z)\sqrt{1 + R_z^2(z)}}{4}$$
$$+ \frac{k_F}{3\pi}\left[1 - \frac{R(z)R_{zz}(z)}{\sqrt{1 + R_z^2(z)}}\right], \quad (13)$$

where $R_z(z) = dR(z)/dz$ and $R_{zz}(z) = d^2R(z)/dz^2$. The second term on the r.h.s. of Eq. (13) is the well-known surface correction in the free-electron model,[19] which compensates for the depletion of surface electrons due to the hard-wall boundary condition. The last term represents an integrated-curvature contribution, which is found to be small correction. The Hartree potential is

$$U(z) = \int_0^L dz'\, V(z, z')\delta\rho(z'), \quad (14)$$

where $\delta\rho(z) = \rho_-(z) - \rho_+(z)$.

Equations (9)–(14) provide a natural, gauge-invariant, generalization of the *nanoscale free-electron model*,[18] which has been successful in describing many equilibrium[17,18] and linear-response[31,32,33] properties of simple metal nanowires, to the case of nanowires at finite bias. This formalism represents a considerable simplification compared to *ab initio* approaches[7,13,14,15,16] or even traditional jellium calculations,[34,35] and permits analytical results for the cohesion and stability of metal nanocylinders at finite bias.

A. Quasicylindrical nanowire without backscattering

Consider a nearly cylindrical nanowire, with radius

$$R(z) = R_0 + \lambda\delta R(z), \quad (15)$$

where λ is a small parameter and $\delta R(z)$ is a slowly-varying function. The couplings of the nanowire to the reservoirs are assumed ideal, so that electrons enter or exit the conductor without backscattering. For sufficiently small λ, electron waves partially reflected or transmitted by the small surface modulation can be neglected. These evanescent modes may exist near the ends of the wire, but will not penetrate into the central section of the wire, if it is sufficiently long. The right(left)-moving electrons in the bulk of the wire are thus in equilibrium with the left(right) reservoir. Moreover, the Hartree potential $U(z)$ varies slowly with z, and can be taken as a shift of the conduction-band bottom in the adiabatic approximation. The injectivity therefore simplifies to

$$g_\alpha(z, E) = \frac{1}{2}g(z, E - U(z)),$$

where $g(z, E)$ is the local density of states for free electrons in a circular slice of radius $R(z)$. Eq. (4) can be

rewritten as

$$\Omega_\alpha[\mu, R(z), U(z)] = \frac{1}{2} \int_0^L dz \int^{\mu-U(z)} dE$$
$$[E - \mu + U(z)] g_T(z, E), \quad (16)$$

where the integration variable E is no longer the total energy of an electron, but rather its kinetic energy. Here $g_T(z, E) = -\int dE' \, g(z, E') \partial f(E - E', 0)/\partial E$ is a convoluted local density of states in a slice of the wire, and can be used to obtain finite-temperature thermodynamic quantities from their zero-temperature expressions,[36] so that Eq. (16) is equivalent to the usual definition of the grand canonical potential (4). Similarly, the linear density of electrons can be written in terms of the convoluted density of states as

$$\rho_-(z) = \frac{\delta\Omega_0}{\delta U(z)} = \frac{1}{2} \sum_{\alpha=\pm} \int^{\mu_\alpha - U(z)} dE \, g_T(z, E). \quad (17)$$

The convoluted density of states of a circular slice of the nanowire can be expressed semiclassically as[36] $g_T(z, E) \equiv \bar{g}_T(z, E) + \delta g_T(z, E)$, where $\bar{g}_T$ is a smoothly-varying function of the geometry, known as the Weyl term, and $\delta g_T(z, E)$ is an oscillatory quantum correction. The temperature dependence of the Weyl term is negligible, $\bar{g}_T = \bar{g} \times \left(1 + \mathcal{O}(T/T_F)^2\right)$, where T_F is the Fermi-temperature. The zero-temperature value is

$$\bar{g}(z, E) = \frac{k_F^3 \partial \mathcal{V}(z)}{2\pi^2 \varepsilon_F} \sqrt{\frac{E}{\varepsilon_F}}$$
$$- \frac{k_F^2 \partial \mathcal{S}(z)}{8\pi \varepsilon_F} + \frac{k_F \partial \mathcal{C}(z)}{6\pi^2 \varepsilon_F} \sqrt{\frac{\varepsilon_F}{E}}, \quad (18)$$

where $\partial \mathcal{V}(z)$, $\partial \mathcal{S}(z)$ and $\partial \mathcal{C}(z)$ are, respectively, the volume, external surface-area, and external mean-curvature of a slice of the wire. The fluctuating part δg_T can be obtained through the trace formula[20]

$$\delta g_T(z, E) = \frac{k_F^2}{2\pi \varepsilon_F} \sum_{wv} f_{vw} a_{vw}(T)$$
$$\times \frac{L_{vw}(z)}{v^2} \cos\theta_{vw}(z, E), \quad (19)$$

where the sum is over all classical periodic orbits (v, w) in a disk billiard[36,37] of radius $R(z)$. Here the factor $f_{vw} = 1$ for $v = 2w$, and 2 otherwise, accounts for the invariance under time-reversal symmetry of some orbits, $L_{vw}(z) = 2vR(z)\sin(\pi w/v)$ is the length of periodic orbit (v, w), $\theta_{vw}(z, E) = k_F L_{vw}(z)\sqrt{E/\varepsilon_F} - 3v\pi/2$, and $a_{vw}(T) = \tau_{vw}/\sinh\tau_{vw}$ is a temperature-dependent damping factor, with $\tau_{vw} = \pi k_F L_{vw} T/2T_F$.

Eqs. (14) and (17) provide a set of self-consistent equations to solve for the ballistic nonequilibrium electron distribution in a quasi-one-dimensional nanoconductor at finite bias. Once the distribution ρ_- is obtained, the grand
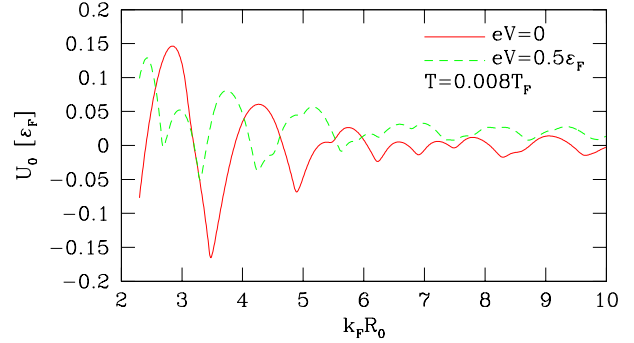

FIG. 2: The Hartree potential U_0 for electrons in a cylindrical nanowire at finite temperature $T = 0.008\,T_F$, with a symmetric potential drop, versus the radius R_0 of the wire.

canonical potential Ω of the electron gas may be calculated from Eqs. (10) and (16). The functional dependence of $\Omega[R(z)]$ yields information on the cohesion[18,19] and stability[20,21,23,38] of a metal nanowire, as in the equilibrium case.

B. Solution for a cylindrical nanowire; Hartree potential and tensile force

For an unperturbed cylinder, the mesoscopic Hartree potential U_0 that simultaneously solves Eqs. (14) and (17) is only a function of the radius R_0, voltage $eV = \mu_+ - \mu_-$, and temperature T, and is constant along the wire (assuming $L < L_{in}$ is long enough for boundary effects to be negligible in most of the wire). U_0 is independent of the choice of η in the Coulomb interaction, Eq. (9), and can be determined by the charge neutrality condition

$$Q = \frac{1}{2}e[N_-(\mu_+ - U_0) + N_-(\mu_- - U_0)] - eN_+ = 0, \quad (20)$$

where $\frac{1}{2}N_-(\mu = \mu_\pm - U_0) = \frac{1}{2}\int_0^L dz \int^\mu dE \, g_T(z, E)$ is the number of right(left)-moving electrons in the cylindrical wire, and N_+ is the total number of background positive charges. Equation (20) gives a relation[12]

$$U_0 = U_0^{(s)}(R_0, V, T) + \frac{1}{2}(\mu_+ + \mu_-) - \varepsilon_F, \quad (21)$$

where $U_0^{(s)}$ is calculated with a symmetric voltage drop $V_+ = -V_- = \frac{1}{2}V$. Equation (21) guarantees that all physical properties of the system calculated in the following are just functions of the voltage V, and not of μ_+ and μ_- separately.

Using these expressions, one can solve Eq. (20) for U_0 for a symmetric potential drop, $\mu_\pm = \varepsilon_F \pm \frac{1}{2}eV$. The solution is shown in Fig. 2 as a function of radius R_0 at two different voltages V. In the equilibrium case ($V = 0$), U_0 oscillates about zero, exhibiting cusps at the subband thresholds, and increasing in amplitude as R_0 decreases,
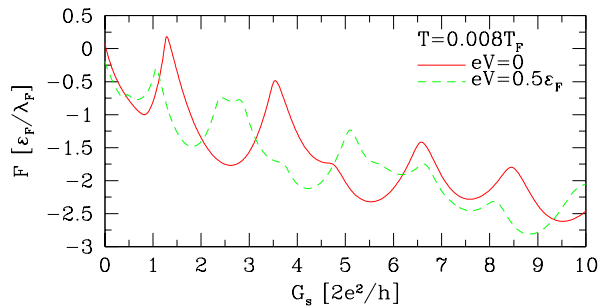
FIG. 3: Tensile force in a metal nanocylinder versus cross-sectional area, at two different bias voltages at temperature $T = 0.008\, T_F$. The cross section is plotted in terms of the Sharvin conductance G_S, Eq. (24), and the force is given in units of ε_F/λ_F (λ_F being the Fermi wavelength), which is 1.7 nN for Au.

due to the quantum confinement. Note that in equilibrium, $U_0 \rightarrow 0$ as $R_0 \rightarrow \infty$, consistent with the well-known behavior of bulk jellium. At finite bias, each cusp in U_0 splits in two, corresponding to the *subband thresholds for left- and right-moving electrons*:

$$\mu_{\pm} = \varepsilon_{\nu}(R_0) + U_0(R_0, V, T), \qquad (22)$$

where $\varepsilon_{\nu}(R_0)$ are the eigenenergies of a disk billiard of radius R_0. This is illustrated in Fig. 2 for $eV = 0.5\varepsilon_F$. Note that in addition to the splitting, there is a substantial shift of the peak structure at finite bias.

Using Eq. (10), the grand canonical potential of a cylinder is now found to be

$$\Omega(R_0, V, T) = \Omega_0[\{\mu_{\pm}\}, R_0, U_0] - N_+ U_0. \qquad (23)$$

Note that Ω is invariant under a global shift of the potential U_0, due to an exact cancellation in the two terms on the r.h.s. of Eq. (23). The tensile force in the nanowire provides direct information about cohesion, and is given by

$$F(R_0, V, T) = -\left.\frac{\partial\Omega}{\partial L}\right|_{R_0^2 L, V, T}.$$

Figure 3 shows the tensile force of a metal nanocylinder as a function of its cross section for two different bias voltages. To facilitate comparison with the stability diagrams in Sec. IV below, the cross section is plotted in terms of the corrected Sharvin conductance[31]

$$G_S = G_0[(k_F R_0/2)^2 - k_F R_0/2], \qquad (24)$$

which gives a semiclassical approximation to the electrical conductance. In Fig. 3, $F < 0$ corresponds to *tension*, while $F > 0$ corresponds to *compression*. As shown below, the cusps in the cohesive force at the subband thresholds correspond to *structural instabilities* of the system.

In Fig. 3, the force calculated at zero bias is very similar to previous results[19,39,40] based on the free-electron

model, even though those calculations did not respect the charge neutrality (20) enforced by Coulomb interactions. The reason for the good agreement is that the contribution of the Hartree potential to the energy of the system is a *second-order* mesoscopic effect at zero bias,[19,24] which is essentially negligible for $G > 3G_0$. An earlier calculation[41] that did invoke charge neutrality obtained a very different—and incorrect—result, because the second term on the r.h.s. of Eq. (23) was omitted, resulting in a double-counting of Coulomb interactions.

Figure 3 shows that the cohesive force of a metal nanowire can be modulated by several nano-Newtons for a bias of a few Volts. Such a large effect should be observable experimentally using appropriate cantilevers,[42,43,44] although the intrinsic behavior might be masked by electrostatic forces in the external circuit. In contrast to the case at $V = 0$, the Coulomb interactions play an essential role in determining the cohesive force at finite bias, since the positions of the peaks depend sensitively on the Hartree potential U_0 of the ballistic nonequilibrium electron distribution, shown in Fig. 2. The gauge-invariant result shown in Fig. 3 thus differs substantially from previous results,[11] where screening was not treated self-consistently. Gauge-invariant results for the nonlinear transport through metal nanocylinders will be presented elsewhere.[45]

IV. LINEAR STABILITY OF A CYLINDER AT FINITE VOLTAGE

In this section, we perform a linear stability analysis[20,21] for cylindrical nanowires under a finite bias V. Coulomb interactions are included self-consistently using the formalism of Sec. III. Although the details of the calculation are rather complicated, the method is conceptually straightforward: Having found the self-consistent solution (23) for a cylinder, we perturb the cylinder as in Eq. (15), and expand the free energy up to second order in the small parameter λ. First, the self-consistent integral equations (14) and (17) for the ballistic nonequilibrium electron distribution are solved using first-order perturbation theory in λ. Then the free energy is calculated using Eqs. (10) and (16).

The radius of the wire is given by Eq. (15), with a perturbation function

$$\delta R(z) = \sum_q b(q)e^{iqz}, \qquad b(q)^* = b(-q).$$

To ensure that the deformation is volume conserving (atoms neither enter nor exit the wire), the coefficient $b(0)$ is fixed by

$$b(0) = -\frac{\lambda}{2R_0}\sum_q |b(q)|^2.$$

The length L of the wire is assumed to be large enough to neglect boundary effects of order $1/L$ on the stability, while still smaller than the inelastic mean-free path.

Within linear response theory, we can expand $\delta\rho(z)$ around U_0 to linear order in $U(z) - U_0$, where U_0 is the mesoscopic Hartree potential for the corresponding unperturbed cylindrical wire. One gets

$$\delta\rho(z) \simeq \delta\rho_0(z) - \int dz' \left.\frac{\delta\rho_-(z)}{\delta U(z')}\right|_{U_0} U_0$$
$$+ \int dz_1 dz_2 \left.\frac{\delta\rho_-(z)}{\delta U(z_1)}\right|_{U_0} V(z_1, z_2)\delta\rho(z_2), \quad (25)$$

where Eq. (14) has been used and $\delta\rho_0(z)$, called the bare charge imbalance, is defined as

$$\delta\rho_0(z) = \frac{1}{2}\sum_{\alpha=\pm}\int^{\mu_\alpha - U_0} dE\, g_T(z, E) - \rho_+(z). \quad (26)$$

Now defining the dielectric function

$$\epsilon(z_1, z_2) = \delta(z_1 - z_2) - \int dz_3 \left.\frac{\delta\rho_-(z_1)}{\delta U(z_3)}\right|_{U_0} V(z_3, z_2), \quad (27)$$

we can rewrite Eq. (25) as

$$\delta\rho(z) = \int dz'\epsilon^{-1}(z, z')\delta\bar{\rho}_0(z'), \quad (28)$$

where ϵ^{-1} is the inverse dielectric function which satisfies $\int dz_3 \epsilon^{-1}(z_1, z_3)\epsilon(z_3, z_2) = \delta(z_1 - z_2)$, and

$$\delta\bar{\rho}_0(z) = \delta\rho_0(z) - \int dz_1 \left.\frac{\delta\rho_-(z)}{\delta U(z_1)}\right|_{U_0} U_0. \quad (29)$$

The functional derivative $\delta\rho_-(z)/\delta U(z')$ can be calculated using Eq. (17), and is found to be

$$\left.\frac{\delta\rho_-(z)}{\delta U(z')}\right|_{U_0} = -\frac{\delta(z - z')}{2}\sum_{\alpha=\pm} g_T(z, \mu_\alpha - U_0).$$

Now we can expand the nonequilibrium grand canonical potential (10) as a series in λ. In order to do so, we first expand Eq. (10) around U_0. Using Eqs. (14), (17), (26) and (29), one gets

$$\Omega = \Omega_0[\{\mu_\pm\}, R(z), U_0] - U_0\int_0^L dz\, \delta\bar{\rho}_0(z)$$
$$+ \frac{1}{2}\int_0^L dz\, dz'\, \delta\bar{\rho}_0(z)\tilde{V}(z, z')\delta\bar{\rho}_0(z')$$
$$+ \frac{(U_0)^2}{4}\sum_{\alpha=\pm}\int_0^L dz\, g_T(z, \varepsilon_\alpha) - N_+ U_0, \quad (30)$$

where $\varepsilon_\pm = \mu_\pm - U_0$, and the screened potential $\tilde{V}(z, z')$ is defined as

$$\tilde{V}(z, z') = \int dz_1 V(z, z_1)\epsilon^{-1}(z_1, z'). \quad (31)$$

At this point, all quantities have been expressed in terms of the local density of states $g_T(z, E)$ and the

Coulomb interaction $V(z, z')$, whose expansions in series of λ are presented in Appendix A. In the end, the expansion of the grand canonical potential as a series in λ is found to be

$$\Omega = \Omega(R_0, V, T) + \lambda^2 L\sum_{q>0}\Xi(q; R_0, V, T)|b(q)|^2 \quad (32)$$

plus terms $\mathcal{O}(\lambda^3)$, where $\Omega(R_0, V, T)$ is given by Eq. (23), and the mode stiffness

$$\Xi(q; R_0, V, T) \equiv \alpha(q; R_0, V, T)$$
$$+ \text{Re}\left(\frac{\hat{V}(q)}{\hat{\epsilon}(q)}\right)(\varrho_1^{(1)} - \varrho_2^{(1)}q^2)^2. \quad (33)$$

Here $\hat{V}(q)$ and $\hat{\epsilon}(q)$ are, respectively, the Fourier transforms of $V^{(0)}(z)$ and $\epsilon^{(0)}(z)$, the Coulomb potential and dielectric function of an unperturbed cylinder. The factors $\varrho_1^{(1)}$ and $\varrho_2^{(1)}$ are given in Eqs. (A6) and (A7). The factor $\alpha(q; R_0, V, T)$ comes from the expansion of $\Omega_0[\{\mu_\pm\}, R(z), U_0]$ and is found to be

$$\alpha(q; R_0, V, T) = -\frac{\pi\sigma_s}{R_0}\frac{\varepsilon_+^2 + \varepsilon_-^2}{\varepsilon_F^2}$$
$$+ \left[\pi\sigma_s R_0\frac{\varepsilon_+^2 + \varepsilon_-^2}{\varepsilon_F^2} - \gamma_s\frac{\varepsilon_+^{3/2} + \varepsilon_-^{3/2}}{\varepsilon_F^{3/2}}\right]q^2$$
$$+ \left(\frac{\partial^2}{\partial R_0^2} - \frac{1}{R_0}\frac{\partial}{\partial R_0}\right)V_{\text{shell}}(R_0, V, T), \quad (34)$$

where σ_s is the surface tension, γ_s is the curvature energy, and $V_{\text{shell}}(R_0, V, T)$ is the mesoscopic *electron-shell potential*,[22] given self-consistently at finite bias by

$$V_{\text{shell}}(R_0, V, T) = \frac{1}{\pi\varepsilon_F}\sum_{\alpha=\pm}\sum_{wv}\frac{a_{vw}(T)f_{vw}}{v^2 L_{vw}}$$
$$\times \varepsilon_\alpha^2 \cos(k_F^\alpha L_{vw} - 3v\pi/2), \quad (35)$$

where $k_F^\pm = k_F\sqrt{\varepsilon_\pm/\varepsilon_F}$. In the present article, the values[18] $\sigma_s = \varepsilon_F k_F^2/16\pi$ and $\gamma_s = 2\varepsilon_F k_F/9\pi^2$ are used throughout. Inserting material-specific values[21] does not lead to a significant change in the stability diagram. Equations (32)–(35) represent the central result of this paper.

A. Stability Diagram

The stability of a cylindrical nanowire of radius R_0 at bias V and temperature T is determined by the function $\Xi(q; R_0, V, T)$: If $\Xi(q) > 0\ \forall q$, then the nanowire is stable with respect to small perturbations, and is a (meta)stable thermodynamic state. If $\Xi(q) < 0$ for any q, then the wire is unstable.

The second term on the r.h.s. of Eq. (33) is positive semidefinite, and thus cannot lead to an instability. The first term $\alpha(q)$ describes instabilities in two different regimes, as in the equilibrium case:[20,21] (*i*) The
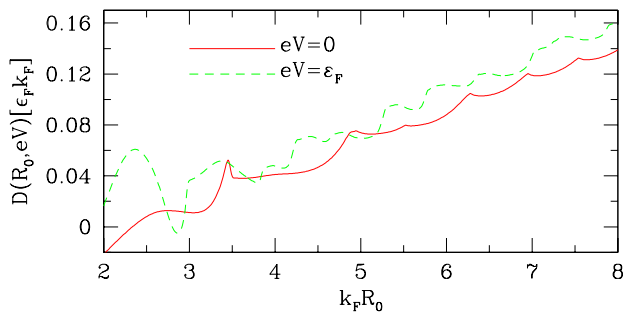
FIG. 4: The factor $D(R_0, V)$, coefficient of the q^2 contribution to $\Xi(q; R_0, V)$, at temperature $T = 0.008\,T_F$.
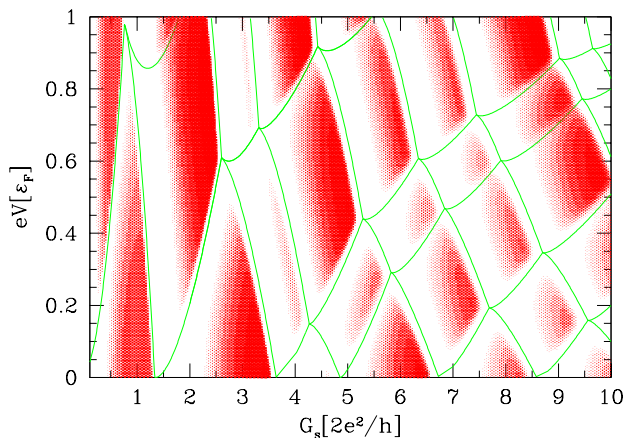

FIG. 5: Stability of cylindrical metal nanowires versus Sharvin conductance (24) and bias voltage. Areas shaded red indicate stability with respect to small perturbations at $T = 0.008\,T_F$. Green lines indicate subband thresholds for right- and left-moving electrons.

electron-shell contribution has deep negative peaks at the thresholds to open new conducting subbands. (ii) The surface contribution to $\alpha(q)$ becomes negative for $qR_0 < 1$, the classical Rayleigh instability. From Eqs. (33) and (34), it is apparent that the most unstable mode (if any) within the semiclassical approximation is $q = 0$, except for unphysical radii $R_0 \lesssim \gamma_s/\sigma_s$ (less than one atom thick). To illustrate this point, the second derivative $D(R_0, V, T) \equiv \partial^2 \Xi / \partial q^2 \big|_{q=0}$ is shown in Fig. 4. Note that $D > 0$ for $k_F R_0 > 3$.

The stability properties of the system are thus completely determined[46] by the sign of the stability function $A(R_0, V, T) \equiv \Xi(q = 0; R_0, V, T)$. Figure 5 shows a stability diagram in the voltage V and radius R_0 plane. The x-axis is given in terms of the Sharvin conductance (24), to facilitate the identification of the quantized (linear-response) conductance values of the stable nanowires. The shaded regions show nanowires that are stable with respect to small perturbations, with darker regions representing larger values of $A(R_0, V, T)$. In the figure, the

solid lines show the subband thresholds for right- and left-moving electrons, which are determined by Eq. (22). At the temperature shown $T = 0.008T_F$, which corresponds roughly to room temperature, the electron-shell effect dominates, leading to instabilities at the subband thresholds, and stabilizing the wire in some of the intervening fingers.

A stability diagram up to $G_S = 50G_0$ is shown in Fig. 6, where the subband thresholds have been omitted to avoid clutter. Figures 5 and 6 show that cylindrical metal nanowires with certain *magic conductance values* $G/G_0 = 1, 3, 6, 12, 17, 23, 34, 42, \ldots$ remain linearly stable at room temperature up to bias voltages $eV \sim 0.1\varepsilon_F$ or higher. These ballistic conductors can therefore support extremely high current densities, of order $10^{11}\mathrm{A/cm^2}$ by Eq. (1). These are precisely the same magic cylinders which were previously found to be linearly stable at zero bias up to very high temperatures.[21] Cylinders with $G/G_0 = 8$ and 10 are also predicted to be stable at finite bias, but not as robust as the neighboring configurations with $G/G_0 = 6$ and 12.

The calculated bias dependence of the stability of metal nanocylinders with conductance $G/G_0 = 1$ and 3, shown in Fig. 5, is consistent with experimental histograms for gold nanocontacts,[2] where a peak at $G \approx G_0$ was found up to 1.9V at room temperature, and a peak at $G \approx 3G_0$ was found up to about 1.5V. Similar experimental results have been obtained by several groups.[3,4,5,6,7,8] It should be mentioned that in addition to the stable cylindrical configurations shown in Figs. 5 and 6, nanowires with elliptical cross sections and conductance $G/G_0 = 2, 5, 9, 29, \ldots$ were also found to be stable at zero bias,[23] although their finite-bias stability has not yet been investigated.

Perhaps the most startling prediction of Figs. 5 and 6 is that there are a number of cylindrical nanowire structures which are stable with respect to small perturbations at finite bias, but unstable in equilibrium! These metastable structures could lead to additional peaks in conductance histograms at finite bias, which are not present at low bias. It may also be possible to observe switching behavior between the various stable structures as the voltage is varied.

B. Nature of the instability

The nature of the predicted instability of metal nanocylinders at finite bias may be illuminated by means of a nontrivial identity[21] linking Eqs. (23) and (33):

$$\lim_{q \to 0} \Xi(q; R_0, V, T) = \left(\frac{\partial^2}{\partial R_0^2} - \frac{1}{R_0} \frac{\partial}{\partial R_0} \right) \frac{\Omega(R_0, V, T)}{L}. \tag{36}$$

This implies that the instability corresponds to a *homogeneous-inhomogeneous transition*,[21] since the r.h.s. of Eq. (36) is proportional to the energetic cost of a volume-conserving phase separation into thick and thin
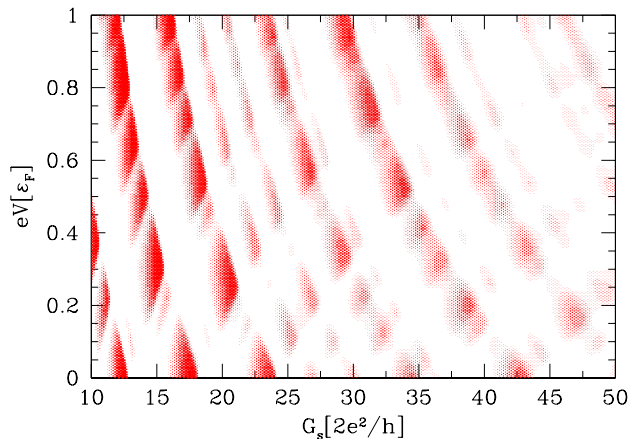
FIG. 6: Stability of cylindrical metal nanowires versus Sharvin conductance G_S between 10 and $50G_0$ and bias voltage. Areas shaded red indicate stability with respect to small perturbations at $T = 0.008\,T_F$.

segments. In the inhomogeneous phase at finite bias, the surface corrugation will not be static, but will diffuse like a defect undergoing *electromigration*.[2,47,48] The stable nanocylinders are immune to electromigration, because they are translationally invariant and they are so thin that they are defect free. Electromigration is possible only if a surface-defect is nucleated,[49] which becomes energetically favorable on the stability boundary. The predicted surface instability may thus represent the ultimate nanoscale limit of electromigration.

V. CONCLUSIONS

In this paper, we develop a self-consistent scattering approach to the nonequilibrium thermodynamics of open mesoscopic systems, and use it to study the cohesion and stability of metal nanocylinders under finite bias. In our approach, the positive ions are modeled as an incompressible fluid, and interactions are treated in the Hartree approximation, using a quasi-one-dimensional form of the Coulomb interaction. This single-band model is appropriate for monovalent metals.

We find that the tensile force in a nanowire can be modulated by several nano-Newtons when biased by a few Volts. Such a large effect should be observable experimentally,[42,43,44] although the intrinsic behavior might be masked by electrostatic forces in the external circuit.

The principal result of this paper is a linear stability analysis of metal nanowires at finite bias, which reveals that cylindrical wires with certain magic conductance values $G/G_0 = 1, 3, 6, 12, 17, 23, 34, 42, \ldots$ remain stable up to bias voltages $eV \sim 0.1\,\varepsilon_F$ or higher, with the maximum sustainable bias decreasing with increasing radius. In particular, wires with $G/G_0 = 1$ and 3 are predicted

to be stable up to $eV \sim 0.5\,\varepsilon_F$, or ~ 2.7 Volts for gold. This maximum voltage is slightly larger than what is observed experimentally.[2,8] It should, however, be pointed out that stability with respect to small perturbations is not a sufficient condition for a nanowire to be observed: Metal nanowires are metastable structures, and can be observed only if their *lifetime* is sufficiently long on the experimental timescale. As a result, the observed maximum sustainable bias is likely to be somewhat smaller than that predicted by a linear stability analysis.

A striking prediction of our stability analysis is the existence of nanowire structures (e.g. cylinders with conductance $G/G_0 = 2, 5, 7, 9, 14, 20, \ldots$) that are only stable under an applied bias. This suggests that conductance histograms taken at finite voltage might have additional peaks, or even a completely different set of peaks, compared to zero-voltage histograms. It may also be possible to observe switching between different stable structures as a function of voltage.

Metal nanowires with elliptical cross sections and conductance $G/G_0 = 2, 5, 9, 29, \ldots$ are also predicted to be stable at zero bias.[23] Although some of the conductance values of the elliptical wires coincide with those of cylindrical wires predicted to be stable only at finite bias, it should be possible to distinguish these geometries experimentally due to the different kinetic pathways involved in their formation, and the very different bias dependence of their stability.

Finally, we point out that the predicted instability of metal nanowires at finite bias may represent the ultimate nanoscale limit of *electromigration*, due to the current-induced nucleation of surface modulation in an otherwise perfect, translationally invariant nanowire.

APPENDIX A: EXPANSION OF THE NON-EQUILIBRIUM FREE ENERGY

In this appendix, we present more details of the derivation of Eqs. (30) and (32).

1. Local Density of States $g_T(z, E)$

In order to include the temperature in the semiclassical formalism, we use a convoluted density of states $g_T(z, E) = \int (-\partial f_0(E - E')/\partial E)\, g(z, E')dE'$, where $f_0(E) = [1 + \exp(\beta E)]^{-1}$. Thermodynamic quantities are then obtained through their zero-temperature expression with the density of states $g(E)$ replaced by $g_T(E)$. The temperature dependence of the average part $\bar{g}_T(z, E)$,

proportional to $(1 + \mathcal{O}(T/T_F)^2) \approx 1$, ($T_F$ is the Fermi temperature), is negligible, while the temperature dependence of the fluctuating part $\delta g_T(z, E)$ is included in the damping factor $a_{vw}(T)$ [see Eq. (19)]. In the following, we set the factor $a_{vw}(T)$ equal to its unperturbed value at the Fermi energy ε_F, since the variation of this factor with the perturbation or with energy does not give an important contribution. We also drop the subscript T for the convoluted density of states to simplify the notation.

For a perturbed cylinder, the average part of the density of states, Eq. (18), can be expanded to second order in the small parameter λ as

$$\bar{g}(z, E) \simeq \bar{g}^{(0)} + \lambda \bar{g}^{(1)} + \lambda^2 \bar{g}^{(2)}, \qquad (A1)$$

where

$$\bar{g}^{(0)} = \frac{k_F^3 R_0^2}{2\pi \varepsilon_F} \sqrt{\frac{E}{\varepsilon_F}} - \frac{k_F^2 R_0}{4\varepsilon_F} + \frac{k_F}{6\pi \varepsilon_F} \sqrt{\frac{\varepsilon_F}{E}},$$

$$\bar{g}^{(1)} = \left[\frac{k_F^3 R_0}{\pi \varepsilon_F} \sqrt{\frac{E}{\varepsilon_F}} - \frac{k_F^2}{4\varepsilon_F} \right] \delta R(z)$$
$$- \frac{k_F R_0}{6\pi \varepsilon_F} \sqrt{\frac{\varepsilon_F}{E}} \delta R''(z),$$

$$\bar{g}^{(2)} = \frac{k_F^3}{2\pi \varepsilon_F} \sqrt{\frac{E}{\varepsilon_F}} \delta R^2(z) - \frac{k_F^2 R_0}{8\varepsilon_F} \delta R'^{\,2}(z)$$
$$- \frac{k_F}{6\pi \varepsilon_F} \sqrt{\frac{\varepsilon_F}{E}} \delta R(z) \delta R''(z),$$

and the prime denotes differentiation with respect to z.

Similarly, the fluctuating part of the density of states for a small deformation of a cylinder, Eq. (19), can be calculated using perturbation semiclassical theory[20,22], and is found to be

$$\delta g(z, E) \simeq \delta g^{(0)}(E) + \lambda \delta g^{(1)}(z, E) + \lambda^2 \delta g^{(2)}(z, E), \quad (A2)$$

with

$$\delta g^{(0)} = \frac{k_F^2}{2\pi \varepsilon_F} \sum_{wv} \frac{a_{vw}(T) f_{vw} L_{vw}}{v^2} \cos \theta_{vw}(E),$$

$$\delta g^{(1)} = \frac{k_F^2}{2\pi \varepsilon_F} \sum_{wv} \frac{a_{vw}(T) f_{vw} L_{vw}}{v^2 R_0} \delta R(z)$$
$$\times [\cos \theta_{vw}(E) - k_E L_{vw} \sin \theta_{vw}(E)],$$

$$\delta g^{(2)} = -\frac{k_F^2}{2\pi \varepsilon_F} \sum_{wv} \frac{a_{vw}(T) f_{vw} L_{vw}^2}{2v^2 R_0^2} k_E \delta R^2(z)$$
$$\times [2 \sin \theta_{vw}(E) + k_E L_{vw} \cos \theta_{vw}(E)].$$

where, once more, the sum is over all classical periodic orbits (v, w) in a disk billiard of radius R_0, the factor $f_{vw} = 1$ for $v = 2w$ and 2 otherwise accounts for the invariance under time-reversal symmetry of some

orbits, $L_{vw} = 2vR_0 \sin(\pi w/v)$ is the length of periodic orbit (v, w), $\theta_{vw}(E) = k_F L_{vw} \sqrt{E/\varepsilon_F} - 3v\pi/2$, and $a_{vw}(T) = \tau_{vw}/\sinh \tau_{vw}$, with $\tau_{vw} = \pi k_F L_{vw} T / 2T_F$, is a temperature dependent damping factor.

To shorten subsequent equations, we define the functions of energy $g_j^{(i)}(E)$ by writing the first- and second-order contributions to the local density of states as

$$g^{(1)}(z, E) = g_1^{(1)}(E) \delta R(z) + g_2^{(1)}(E) \delta R''(z), \quad (A3)$$

$$g^{(2)}(z, E) = g_1^{(2)}(E) \delta R^2(z) + g_2^{(2)}(E) \delta R'^{\,2}(z)$$
$$+ g_3^{(2)}(E) \delta R(z) \delta R''(z). \quad (A4)$$

The total density of states per unit length of a cylindrical wire is $g^{(0)}(E) = \bar{g}^{(0)}(E) + \delta g^{(0)}(E)$.

2. Bare charge imbalances $\delta \rho_0(z)$ and $\delta \bar{\rho}_0(z)$

Now substituting the expansion of the local density of states into Eq. (26), one gets the expansion of $\delta \rho_0(z)$ as

$$\delta \rho_0(z) \simeq \lambda \delta \rho_0^{(1)} + \lambda^2 \delta \rho_0^{(2)}, \qquad (A5)$$

with

$$\delta \rho_0^{(1)}(z) = \varrho_1^{(1)} \delta R(z) + \varrho_2^{(1)} \delta R''(z),$$

where the coefficients $\varrho_1^{(1)}$ and $\varrho_2^{(1)}$ are defined as

$$\varrho_1^{(1)} = \frac{k_F^3 R_0}{3\pi} \left[\frac{\varepsilon_+^{3/2} + \varepsilon_-^{3/2}}{\varepsilon_F^{3/2}} - 2 \right]$$
$$- \frac{k_F^2}{8} \left[\frac{\varepsilon_+ + \varepsilon_-}{\varepsilon_F} - 2 \right] + \frac{\delta \varrho_+^{(1)} + \delta \varrho_-^{(1)}}{2}, \quad (A6)$$

$$\varrho_2^{(1)} = -\frac{k_F R_0}{6\pi} \left[\frac{\varepsilon_+^{1/2} + \varepsilon_-^{1/2}}{\varepsilon_F^{1/2}} - 2 \right], \qquad (A7)$$

with $\varepsilon_\pm = \mu_\pm - U_0$, and

$$\delta \varrho_\pm^{(1)} = \frac{k_F^2 \varepsilon_\pm}{\pi \varepsilon_F} \sum_{vw} \frac{f_{vw} a_{vw}(T)}{v^2 R_0} L_{vw}$$
$$\times \left(\cos \theta_{vw}(\varepsilon_\pm) + \frac{1}{k_F^\pm L_{vw}} \sin \theta_{vw}(\varepsilon_\pm) \right),$$

where $k_F^\pm = k_F \sqrt{\varepsilon_\pm / \varepsilon_F}$, while

$$\delta \rho_0^{(2)}(z) = \varrho_1^{(2)} \delta R^2(z) + \varrho_2^{(2)} \delta R'^{\,2}(z) + \varrho_3^{(2)} \delta R(z) \delta R''(z),$$

where coefficients $\varrho_1^{(2)}$, $\varrho_2^{(2)}$ and $\varrho_3^{(2)}$ are

$$\varrho_1^{(2)} = \frac{k_F^3}{6\pi} \left[\frac{\varepsilon_+^{3/2} + \varepsilon_-^{3/2}}{\varepsilon_F^{3/2}} - 2 \right] + \frac{\delta \varrho_+^{(2)} + \delta \varrho_-^{(2)}}{2},$$

$$\varrho_2^{(2)} = -\frac{k_F^2 R_0}{16} \left[\frac{\varepsilon_+ + \varepsilon_-}{\varepsilon_F} - 2 \right], \quad \varrho_3^{(2)} = \frac{\varrho_2^{(1)}}{R_0},$$

and

$$\delta\varrho_\pm^{(2)} = -\frac{k_F^2}{2\pi}\frac{\varepsilon_\pm}{\varepsilon_F}\sum_{vw}\frac{f_{vw}a_{vw}(T)}{v^2 R_0^2}L_{vw}^2$$

$$\times\left(\sin\theta_{vw}(\varepsilon_\pm) - \frac{2}{k_F^\pm L_{vw}}\cos\theta_{vw}(\varepsilon_\pm)\right).$$

Similarly, Eq. (29) for $\delta\bar\rho_0(z)$ is expanded as

$$\delta\bar\rho_0(z,E) \simeq \delta\bar\rho_0^{(0)} + \lambda\delta\bar\rho_0^{(1)} + \lambda^2\delta\bar\rho_0^{(2)}, \qquad (A8)$$

with

$$\delta\bar\rho_0^{(0)} = \frac{U_0}{2}\left[g^{(0)}(\varepsilon_+) + g^{(0)}(\varepsilon_-)\right],$$
$$\delta\bar\rho_0^{(1)} = \bar\varrho_1^{(1)}\delta R(z) + \bar\varrho_2^{(1)}\delta R''(z),$$
$$\delta\bar\rho_0^{(2)} = \bar\varrho_1^{(2)}\delta R^2(z) + \bar\varrho_2^{(2)}\delta R'^2(z) + \bar\varrho_3^{(2)}\delta R(z)\delta R''(z),$$

where $\bar\varrho_j^{(i)} \equiv \varrho_j^{(i)} + \frac{1}{2}U_0[g_j^{(i)}(\varepsilon_+) + g_j^{(i)}(\varepsilon_-)]$.

3. Effective Coulomb potential $V(z,z')$

The expansion of the Coulomb potential (9) as a series in λ gives

$$V(z,z') \simeq V^{(0)}(z-z')$$
$$+ \lambda V^{(1)}(z,z') + \lambda^2 V^{(2)}(z,z'), \quad (A9)$$

where

$$V^{(0)}(z) = \frac{e^2}{\sqrt{z^2 + \eta R_0^2}},$$

$$V^{(1)}(z,z') = \frac{\delta R(z) + \delta R(z')}{2}\cdot\frac{dV^{(0)}(z-z')}{dR_0},$$

$$V^{(2)}(z,z') = \frac{1}{8}\left([\delta R(z) + \delta R(z')]^2\frac{d}{dR_0}\right.$$
$$\left.+\frac{[\delta R(z) - \delta R(z')]^2}{R_0}\right)\frac{dV^{(0)}(z-z')}{dR_0}.$$

For future use, let us define the Fourier transform of $V^{(0)}(z)$ as

$$\hat V(q) = \int_0^L dz\, e^{-iqz}V^{(0)}(z). \qquad (A10)$$

Note that $\mathrm{Re}\hat V(q) > 0$.

4. Inverse dielectric function $\epsilon^{-1}(z,z')$

We first expand the dielectric function $\epsilon(z,z')$, Eq. (27), as

$$\epsilon(z,z') = \epsilon^{(0)}(z-z')$$
$$+ \lambda\epsilon^{(1)}(z,z') + \lambda^2\epsilon^{(2)}(z,z'), \quad (A11)$$

where the zeroth-order term is

$$\epsilon^{(0)}(z) = \delta(z) + \frac{g^{(0)}(\varepsilon_+) + g^{(0)}(\varepsilon_-)}{2}V^{(0)}(z), \quad (A12)$$

the first-order term is

$$\epsilon^{(1)}(z,z') = \frac{1}{2}\sum_{\alpha=\pm}\left(g^{(1)}(z,\varepsilon_\alpha)V^{(0)}(z-z')\right.$$
$$\left.+ g^{(0)}(z,\varepsilon_\alpha)V^{(1)}(z,z')\right),$$

and the second-order term is

$$\epsilon^{(2)}(z,z') = \frac{1}{2}\sum_{\alpha=\pm}\left(g^{(2)}(z,\varepsilon_\alpha)V^{(0)}(z-z')\right.$$
$$\left.+ g^{(1)}(z,\varepsilon_\alpha)V^{(1)}(z,z') + g^{(0)}(z,\varepsilon_\alpha)V^{(2)}(z,z')\right).$$

Let us define the Fourier transform of $\epsilon^{(0)}(z)$ as

$$\hat\epsilon(q) = \int_0^L dz\, e^{-iqz}\epsilon^{(0)}(z)$$
$$= 1 + \frac{g^{(0)}(\varepsilon_+) + g^{(0)}(\varepsilon_-)}{2}\hat V(q). \qquad (A13)$$

Note that $\mathrm{Re}\left(\hat\epsilon(q)/\hat V(q)\right) > 0$, since both $g^{(0)}(\varepsilon) > 0$ and $\hat V(q) > 0$. Substituting Eq. (A11) into the identity

$$\int dz''\,\epsilon^{-1}(z,z'')\epsilon(z'',z') = \delta(z-z'),$$

one can solve order by order for the inverse dielectric function $\epsilon^{-1}(z,z')$

$$\epsilon^{-1}(z,z') = \epsilon^{-1,(0)}(z-z')$$
$$+ \lambda\epsilon^{-1,(1)}(z,z') + \lambda^2\epsilon^{-1,(2)}(z,z'), \quad (A14)$$

where the zeroth-order term is

$$\epsilon^{-1,(0)}(z) = \frac{1}{L}\sum_q\frac{e^{iqz}}{\hat\epsilon(q)},$$

the first-order term is found to be

$$\epsilon^{-1,(1)} = -\int dz_1\int dz_2\,\epsilon^{-1,(0)}(z-z_1)$$
$$\times \epsilon^{(1)}(z_1,z_2)\,\epsilon^{-1,(0)}(z_2-z'),$$

and the second-order term is

$$\epsilon_j^{-1,(2)}(z,z') = -\int dz_1\int dz_2\,\epsilon^{-1,(0)}(z_2-z')$$
$$\times\left[\epsilon^{-1,(0)}(z-z_1)\,\epsilon_j^{(2)}(z_1,z_2)\right.$$
$$\left.+ \epsilon^{-1,(1)}(z-z_1)\,\epsilon_j^{(1)}(z_1,z_2)\right].$$

5. Screened Potential $\tilde{V}(z,z')$

Substituting the expansions (A9) and (A14) of V and ϵ^{-1} into Eq. (31), one gets an expansion of the screened potential as

$$\tilde{V}(z,z') = \tilde{V}^{(0)}(z-z')$$
$$+ \lambda\,\tilde{V}^{(1)}(z,z') + \lambda^2\,\tilde{V}^{(2)}(z,z') \quad (A15)$$

where the zeroth-order term is

$$\tilde{V}^{(0)}(z) = \int dz_1\, V^{(0)}(z-z_1)\epsilon^{-1,(0)}(z_1) = \frac{1}{L}\sum_q \frac{\hat{V}(q)}{\hat{\epsilon}(q)}e^{iqz},$$

the first-order term is

$$\tilde{V}^{(1)}(z,z') = \int dz_1\Big[V^{(0)}(z-z_1)\epsilon^{-1,(1)}(z_1,z')$$
$$+ V^{(1)}(z-z_1)\epsilon^{-1,(0)}(z_1-z')\Big],$$

while the second-order term is

$$\tilde{V}^{(2)}(z,z') = \int dz_1\Big[V^{(0)}(z-z_1)\epsilon^{-1,(2)}(z_1,z')$$
$$+ V^{(1)}(z-z_1)\epsilon^{-1,(1)}(z_1,z')$$
$$+ V^{(2)}(z-z_1)\epsilon^{-1,(0)}(z_1-z')\Big].$$

6. Grand canonical potential $\Omega[V,R(z),U(z)]$

Using Eqs. (A1, A2, A5, A8, A15) for $g(z,E)$, $\delta\rho_0$, $\delta\bar{\rho}_0$, and $\tilde{V}$, we are now ready to expand Ω, starting by rewriting Eq. (30) as

$$\Omega \simeq \Omega_0[\{\mu_\pm\},R(z),U_0] - N_+U_0$$
$$- \Omega_1[\{\mu_\pm\},R(z),U_0] + \Omega_2[\{\mu_\pm\},R(z),U_0]$$
$$+ \Omega_3[\{\mu_\pm\},R(z),U_0], \quad (A16)$$

where

$$\Omega_1 = U_0\int dz\,\delta\bar{\rho}_0(z)$$
$$= U_0 L\Big[\frac{U_0}{2}\sum_{\alpha=\pm} g^{(0)}(\varepsilon_\alpha) + \lambda\bar{\varrho}_1^{(1)}b(0)$$
$$+ \lambda^2\sum_q \Big[\bar{\varrho}_1^{(2)} + (\bar{\varrho}_2^{(2)} - \bar{\varrho}_3^{(2)})q^2\Big]|b(q)|^2\Big],$$

$$\Omega_2 = \frac{(U_0)^2}{4}\sum_{\alpha=\pm}\int dz\,g(z,\varepsilon_\alpha)$$
$$= \frac{(U_0)^2}{4}L\sum_{\alpha=\pm}\Big[g^{(0)}(\varepsilon_\alpha) + \lambda g_1^{(1)}(\varepsilon_\alpha)b(0)$$
$$+ \lambda^2\sum_q \Big[g_1^{(2)}(\varepsilon_\alpha) + [g_2^{(2)}(\varepsilon_\alpha) - g_3^{(2)}(\varepsilon_\alpha)]q^2\Big]|b(q)|^2\Big],$$

and $\Omega_3 = \frac{1}{2}\int dz dz'\delta\bar{\rho}_0(z)\tilde{V}(z,z')\delta\bar{\rho}_0(z)$ can be written as

$$\Omega_3[\{\mu_\pm\},R(z),U_0] = \Omega_3^{(0)}[\{\mu_\pm\},R_0,U_0]$$
$$+ \lambda\,\Omega_3^{(1)}[\{\mu_\pm\},R_0,U_0] + \lambda^2\,\Omega_3^{(2)}[\{\mu_\pm\},R_0,U_0].$$

The zero-th order term in the expansion of Ω_3 is

$$\Omega_3^{(0)} = \frac{1}{2}\int dz dz'\,\delta\bar{\rho}_0^{(0)}(z)\tilde{V}^{(0)}(z-z')\delta\bar{\rho}_0^{(0)}(z')$$
$$= \frac{L}{4}(U_0)^2\sum_{\alpha=\pm} g^{(0)}(\varepsilon_\alpha),$$

the first-order term is

$$\Omega_3^{(1)} = \frac{1}{2}\int dz dz'\Big[\delta\bar{\rho}_0^{(0)}(z)\tilde{V}^{(1)}(z,z')\delta\bar{\rho}_0^{(0)}(z')$$
$$+ 2\delta\bar{\rho}_0^{(1)}(z)\tilde{V}^{(0)}(z-z')\delta\bar{\rho}_0^{(0)}(z')\Big]$$
$$= LU_0\bar{\varrho}_1^{(1)}b(0) + \mathcal{O}(L^0),$$

and the second-order contribution is

$$\Omega_3^{(2)} = \frac{1}{2}\int dz dz'\Big[\delta\bar{\rho}_0^{(0)}(z)\tilde{V}^{(2)}(z,z')\delta\bar{\rho}_0^{(0)}(z')$$
$$+ 2\delta\bar{\rho}_0^{(0)}(z)\tilde{V}^{(1)}(z,z')\delta\bar{\rho}_0^{(1)}(z')$$
$$+ 2\delta\bar{\rho}_0^{(2)}(z)\tilde{V}^{(0)}(z-z')\delta\bar{\rho}_0^{(0)}(z')$$
$$+ \delta\bar{\rho}_0^{(1)}(z)\tilde{V}^{(0)}(z-z')\delta\bar{\rho}_0^{(1)}(z')\Big]$$
$$= LU_0\sum_q \Big[\varrho_1^{(2)} + (\varrho_2^{(2)} - \varrho_3^{(2)})q^2\Big]|b(q)|^2$$
$$+ \frac{L}{2}\sum_q \frac{\hat{V}(q)}{\hat{\epsilon}(q)}\Big[\varrho_1^{(1)} - \varrho_2^{(1)}q^2\Big]^2|b(q)|^2 + \mathcal{O}(L^0).$$

Adding up all the contributions in Eq. (A16), and dropping contributions of order L^0, one gets Eqs. (32) and (33).

The above calculations also show that Eq. (30) can be rewritten as

$$\Omega = \Omega_0[\{\mu_\pm\},R(z),U_0] - N_+U_0$$
$$+ \frac{1}{2}\int dz dz'\,\delta\rho_0^{(1)}(z)\tilde{V}^{(0)}(z-z')\delta\rho_0^{(1)}(z')$$
$$+ \mathcal{O}(L^0). \quad (A17)$$

[1] N. Agraït, A. Levy Yeyati, and J. M. van Ruitenbeek, Phys. Rep. **377**, 81 (2003).

[2] H. Yasuda and A. Sakai, Phys. Rev. B **56**, 1069 (1997).

[3] K. Itakura, K. Yuki, S. Kurokawa, H. Yasuda, and A. Sakai, Phys. Rev. B **60**, 11163 (1999).

[4] C. Untiedt, G. Rubio Bollinger, S. Vieira, and N. Agraít, Phys. Rev. B **62**, 9962 (2000).

[5] K. Hansen, S. K. Nielsen, M. Brandbyge, E. Lægsgaard, I. Stensgaard, and F. Besenbacher, Appl. Phys. Lett. **77**, 708 (2000).

[6] K. Yuki, A. Enomoto, and A. Sakai, Appl. Surf. Sci. **169–170**, 489 (2001).

[7] H. Mehrez, A. Wlasenko, B. Larade, J. Taylor, P. Grutter, and H. Guo, Phys. Rev. B **65**, 195419 (2002).

[8] N. Agraït, C. Untiedt, G. Rubio-Bollinger, and S. Vieira, Phys. Rev. Lett. **88**, 216803 (2002).

[9] J. I. Pascual, J. A. Torres, and J. J. Sáenz, Phys. Rev. B **55**, 16029 (1997).

[10] E. N. Bogacheck, A. G. Scherbakov, and U. Landman, Phys. Rev. B **56**, 14917 (1997).

[11] A. M. Zagoskin, Phys. Rev. B **58**, 15827 (1998).

[12] T. Christen and M. Büttiker, Europhys. Lett. **35**, 523 (1996).

[13] T. N. Todorov, J. Hoekstra, and A. P. Sutton, Phil. Mag. B **80**, 421 (2000).

[14] M. Di Ventra and N. D. Lang, Phys. Rev. B **65**, 045402 (2002).

[15] M. Brandbyge, J.-L. Mozos, P. Ordejón, J. Taylor, and K. Stokbro, Phys. Rev. B **65**, 165401 (2002).

[16] J. L. Mozos, P. Ordejón, M. Brandbyge, J. Taylor, and K. Stokbro, Nanotechnology **13**, 346 (2002).

[17] D. F. Urban, J. Bürki, A. I. Yanson, I. K. Yanson, C. A. Stafford, J. M. van Ruitenbeek, and H. Grabert, Solid State Comm. **131**, 609 (2004).

[18] C. A. Stafford, D. Baeriswyl, and J. Bürki, Phys. Rev. Lett. **79**, 2863 (1997).

[19] C. A. Stafford, F. Kassubek, J. Bürki, and H. Grabert, Phys. Rev. Lett. **83**, 4836 (1999).

[20] F. Kassubek, C. A. Stafford, H. Grabert, and R. E. Goldstein, Nonlinearity **14**, 167 (2001).

[21] C.-H. Zhang, F. Kassubek, and C. A. Stafford, Phys. Rev. B **68**, 165414 (2003).

[22] J. Bürki, R. E. Goldstein, and C. A. Stafford, Phys. Rev. Lett. **91**, 254501 (2003).

[23] D. F. Urban, J. Bürki, C.-H. Zhang, C. A. Stafford, and H. Grabert, Phys. Rev. Lett. **93**, 186403 (2004).

[24] C. A. Stafford, F. Kassubek, J. Bürki, H. Grabert, and D. Baeriswyl, in *Quantum Physics at the Mesoscopic Scale*, edited by D. C. Glattli, M. Sanquer, and J. Tran Thanh Van (EDP Sciences, Les Ulis, France, 2000), pp. 445–449.

[25] C. A. Stafford, F. Kassubek, and H. Grabert, in *Advances in Solid State Physics*, edited by B. Kramer (Springer-Verlag, Berlin Heidelberg, 2001), pp. 497–511.

[26] T. Christen, Phys. Rev. B **55**, 7606 (1996).

[27] M. Büttiker, J. Phys. Condens. Matter **5**, 9361 (1993).

[28] V. Gasparian, T. Christen, and M. Büttiker, Phys. Rev. A **54**, 4022 (1996).

[29] Other choices for the transverse confinement potential[30] lead to qualitatively similar results.

[30] A. Garcia-Martin *et al.*, Phys. Rev. B **54**, 13448 (1996).

[31] J. A. Torres, J. I. Pascual, and J. J. Sáenz, Phys. Rev. B **49**, 16581 (1994).

[32] J. Bürki, C. A. Stafford, X. Zotos, and D. Baeriswyl, Phys. Rev. B **60**, 5000 (1999).

[33] J. Bürki and C. A. Stafford, Phys. Rev. Lett. **83**, 3342 (1999).

[34] C. Yannouleas, E. N. Bogachek, and U. Landman, Phys. Rev. B **57**, 4872 (1998).

[35] M. J. Puska, E. Ogando, and N. Zabala, Phys. Rev. B **64**, 033401 (2001).

[36] M. Brack and R. K. Bhaduri, *Semiclassical Physics* (Addison-Wesley, Reading, MA, 1997).

[37] R. Balian and C. Bloch, Ann. Phys. (N. Y.) **69**, 76 (1972).

[38] D. F. Urban and H. Grabert, Phys. Rev. Lett. **91**, 256803 (2003).

[39] S. Blom *et al.*, Phys. Rev. B **57**, 8830 (1998).

[40] C. Höppler and W. Zwerger, Phys. Rev. B **59**, R7849 (1999).

[41] J. M. van Ruitenbeek, M. H. Devoret, D. Esteve, and C. Urbina, Phys. Rev. B **56**, 12566 (1997).

[42] C. Rubio, N. Agraït, and S. Vieira, Phys. Rev. Lett. **76**, 2302 (1996).

[43] A. Stalder and U. Dürig, Appl. Phys. Lett. **68**, 637 (1996).

[44] G. Rubio-Bollinger, P. Joyez, and N. Agrait, Phys. Rev. Lett. **93**, 116803 (2004).

[45] C.-H. Zhang, unpublished.

[46] A short-wavelength Peierls instability also arises in a fully quantum-mechanical treatment,[38] but only at very low temperatures.

[47] K. S. Ralls, D. C. Ralph, and R. A. Buhrman, Phys. Rev. B **40**, 11561 (1989).

[48] C. Höppler and W. Zwerger, Phys. Rev. B **45**, 9311 (1992).

[49] J. Bürki, C. A. Stafford, and D. L. Stein, in *Noise in Complex Systems and Stochastic Dynamics II*, edited by Z. Gingl et al. (SPIE Proceedings, 2004), vol. 5471, pp. 367–379.